Design of three-dimensional domain-swapped dimers and fibrous oligomers

Nancy L. Ogihara*†‡, Giovanna Ghirlanda§, James W. Bryson§¶, Mari Gingery†, William F. DeGrado§, and David Eisenberg*†‖

*UCLA-DOE Laboratory of Structural Biology and the Department of Chemistry and Biochemistry, P.O. Box 951570, University of California, Los Angeles, CA 90095-1570; §The Johnson Research Foundation, Department of Biochemistry and Biophysics, University of Pennsylvania School of Medicine, Philadelphia, PA 19104-6059; and †Molecular Biology Institute, Box 951570, University of California, Los Angeles, CA 90095-1570

Contributed by William F. DeGrado, December 4, 2000

Three-dimensional (3D) domain-swapped proteins are intermolecularly folded analogs of monomeric proteins; both are stabilized by the identical interactions, but the individual domains interact intramolecularly in monomeric proteins, whereas they form intermolecular interactions in 3D domain-swapped structures. The structures and conditions of formation of several domain-swapped dimers and trimers are known, but the formation of higher order 3D domain-swapped oligomers has been less thoroughly studied. Here we contrast the structural consequences of domain swapping from two designed three-helix bundles: one with an up-down-up topology, and the other with an up-down-down topology. The up-down-up topology gives rise to a domain-swapped dimer whose structure has been determined to 1.5 Å resolution by x-ray crystallography. In contrast, the domain-swapped protein with an up-down-down topology forms fibrils as shown by electron microscopy and dynamic light scattering. This demonstrates that design principles can predict the oligomeric state of 3D domain-swapped molecules, which should aid in the design of domain-swapped proteins and biomaterials.

Three-dimensional (3D) domain swapping is a mechanism of exchanging one structural domain of a protein monomer with that of the identical domain from a second monomer, resulting in an intertwined oligomer. The swapped domain has nearly identical noncovalent interactions in the oligomer as in the monomer. More than a dozen crystal structures have been determined of dimers and trimers that are 3D domain swapped (1). Domain swapping provides a plausible mechanism for the evolution of functional sites located between the monomeric units of oligomers with well-defined aggregation states (2). 3D domain swapping may also lead to polymerization, and has been suggested as a mechanism of forming protein amyloid fibrils (1, 3). At least two proteins, diphtheria toxin and ribonuclease A, are known to form higher order oligomers (4–6), but the atomic structures of these oligomers are not yet known. These oligomers form under the same conditions as the 3D domain-swapped dimers (DSDs) of known structure, and are presumably also linked by swapping domains.

The present paper illustrates through protein design how 3D domain swapping can lead to a DSD or to domain-swapped oligomers, depending on the topology of the monomeric protein. To illustrate this concept, we have prepared domain-swapped derivatives of two different, monomeric 3-helix bundles (Fig. 1 *A* and *B*). The bundles (Fig. 1) are variants of the designed 3-α-helical bundle called coil-Ser, whose design (7–9) was based on the heptad repeat sequence of α-helical coiled coils. The 3-α-helical bundle of coil-Ser has an antiparallel packing arrangement, in which each α-helix is made of four heptad repeats containing leucine residues in the *a* and *d* heptad positions (Fig. 1*C*; ref. 10). The crystallographically determined structure of coil-Ser has served as a template for the design of antiparallel three-α-helix bundles with up-down-up topologies, consisting of three α-helices interconnected by two short loops (11–13). In these designs, the helices were shortened to a length of three heptads, and interhelical electrostatic interactions (14) were used to define a unique topology. Here, we examine domain-swapped versions of this class of three-α-helix bundle proteins. To simplify the synthesis and modeling, the helices in the target structures were further shortened to two heptads, resulting in a model three-helix bundle with 14 residues per helix. The helices were then connected by loops to provide two bundles differing in topology, designated Mon1 and Mon2, with up-down-up (Fig. 1*A*) and up-down-down (Fig. 1*B*) topologies, respectively.

Loop deletion is a common mechanism for forming 3D domain-swapped oligomers from monomers, and is seen in a number of natural proteins (15–18). We therefore considered the consequences of deleting the second hairpin loop (Loop 2), which should give rise to a hairpin shaped open monomer with a short 14-residue α-helix (domain I) packed antiparallel against a longer, 28-residue α-helix (comprising domains II and III) (Fig. 1 *A* and *B*). Depending on the topology of the starting bundle, the oligomerization of the resulting open monomers should lead to different results. If the original closed monomeric protein has an up-down-up topology, domains I and II from one open monomer might be expected to interact with domain III′ of a second open monomer, with retention of the up-down-up topology. This topology allows the same type of interaction, as seen in Mon1, between domains I′/II′ and domain III, resulting in a "closed" DSD containing two "functional units" (19), each an up-down-up three-α-helix bundle (Figs. 1*A* and 2). By contrast, with an up-down-down topology (Fig. 1*B*) the association of domains I/II of the first monomer with domain III′ of a second monomer leads to a structure in which domains I′/II′ and III protrude from opposite ends of the functional unit. These "sticky" end-sequences would be expected to associate further with other open monomeric units by forming three-helix bundles and leading to a multimeric fibrous assembly.

The above considerations suggest that a domain-swapped up-down-up three-α-helix bundle will form a closed, dimeric structure, whereas an up-down-down construct will tend to form open, fibrous oligomers.

Materials and Methods

Synthesis and Purification. Peptides were synthesized and purified as described (20). Their molecular weights were verified by matrix-assisted laser desorption mass spectrometry.

Abbreviations: CD, circular dichroism; DSD, domain-swapped dimer; DSAg, domain-swapped aggregate; Gdn·HCl, guanidine hydrochloride; 3D, three-dimensional.

Data deposition: The atomic coordinates have been deposited in the Protein Data Bank, www.rcsb.org (PDB ID code 1g6u).

‡Present address: Molecular Simulations, 9685 Scranton Road, San Diego, CA 92121.

¶Present address: Bristol-Myers Squibb Company, Mail Stop H13-05, P.O. Box 4000, Princeton, NJ 08543-4000.

‖To whom reprint requests should be addressed. E-mail: david@mbi.ucla.edu.

The publication costs of this article were defrayed in part by page charge payment. This article must therefore be hereby marked "*advertisement*" in accordance with 18 U.S.C. §1734 solely to indicate this fact.

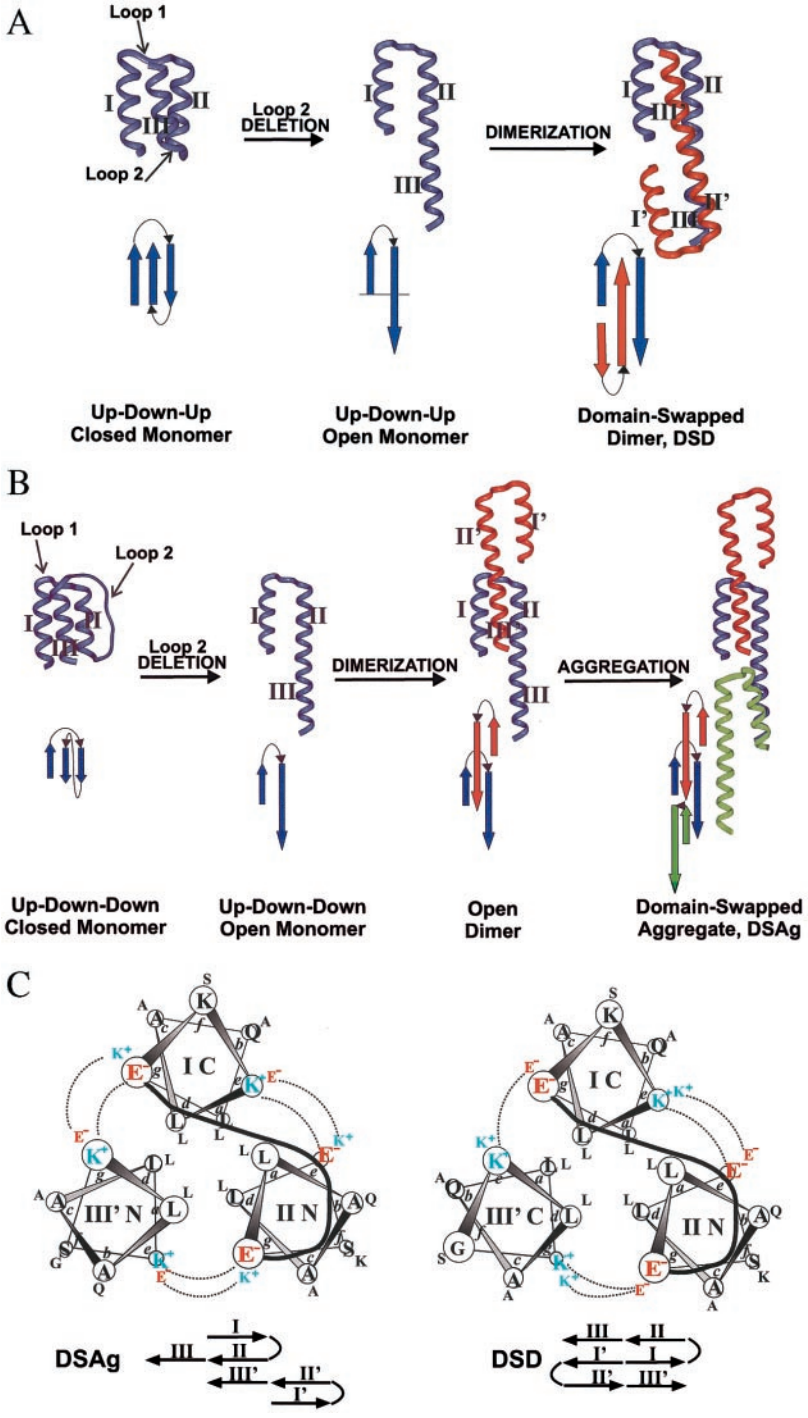

Fig. 1. Design of up-down-up and up-down-down three-helix bundles, and their domain-swapped counterparts. (*A*) Design of a DSD, beginning with Mon1 (up-down-up topology). (*B*) Design of a domain-swapped open aggregate, starting with Mon2 (up-down-down topology). (*C*) Helical wheel diagrams and amino acid sequence of DSAg and DSD. Each helical wheel diagram illustrates a single functional unit. The topologies of the functional units of DSAg and DSD differ only with respect to the orientation of helix III′ (antiparallel to helix I in DSAg and parallel in DSD). The positions of the Glu and Lys residues at the helix interfaces have been arranged to differentially stabilize the two different topologies. Notice that the leucine-containing hydrophobic cores are identical. In the amino acid sequences of DSD and DSAg, the leucine core (*a* and *d* heptad positions) are the same. Only the charged *e* and *g* positions are redistributed to reorient the molecules.

Electron Microscopy. Samples were prepared for electron microscopy by dissolving lyophilized protein powder to a concentration of 12.5 mg/ml in either 50 mM Mes (pH 6.5) or in 50 mM Acetic (pH 2.4). Protein solutions were held at room temperature for 30 min, then filtered through a 0.1-μm pore size Anodisc (Whatman) membrane. The filtrate was held for an additional 15 min at room temperature before application to grids.

Carbon-coated parlodion support films mounted on copper grids were made hydrophilic immediately before use by high voltage alternating current glow discharge. Samples were applied directly onto grids and allowed to adhere for 2 min. Grids were rinsed with distilled water and negatively stained with 1% uranyl acetate. Specimens were examined in an H-7000 (Hitachi, Tokyo) telectron microscope at an accelerating voltage of 75 kV.

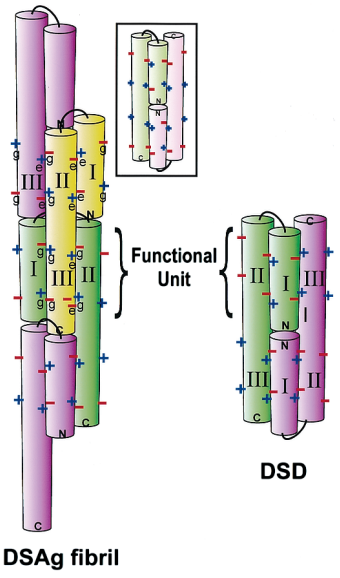

Fig. 2. The designed *e–g* salt bridges stabilizing the conformations for DSD and DSAg. + indicates a positively charged Lys side chain; − indicates a negatively charged Glu side chain. Colored cylinders represent the α-helical domains. Notice DSD contains only two functional units, and the DSAg fibril can contain an unlimited number of functional units because the C-terminal domain of each monomer is always available to bind an additional molecule.

Dynamic Light Scattering. Dynamic light scattering was performed on a DynaPro MS (microsampler) (Protein Solutions, Charlottesville, VA) dynamic light scattering instrument using the DYNAMICS V4.0 software from Protein Solutions. Samples were prepared by dissolving purified, lyophilized samples of DSD or domain-swapped aggregate (DSAg) in 50 mM Mes (pH 6.5) or 50 mM Acetic acid (pH 2.4) to a concentration of 7.3 mg/ml. Samples incubated for 35 min before filtering through a 0.1-μm Anodisc (Whatman) membrane and taking measurements.

Crystallization. Crystallization and data collection: Crystals of DSD grew from 2.6 M ammonium sulfate, 100 mM Mes (pH 6.5), 100 mM NaCl, and 1% dioxane. X-ray diffraction data for both native and derivative crystals were collected at room temperature by using an RAXIS IIC imaging plate detector system with CuKα radiation and a monochromator from a Rigaku RU-200B (Tokyo) generator operated at 50 kV and 100 mA. The crystal to detector distance was 100 mm, and crystals were rotated about the spindle axis with oscillation images collected in sweeps of 2°. Native synchrotron data were collected at −180°C at Brookhaven National Laboratory beamline X12B where the x-ray wavelength was tuned to 0.975 Å. The crystal-to-detector distance was 188 mm. Crystals were rotated about the spindle axis with oscillations collected in sweeps of 2°. All x-ray diffraction data were processed to 1.5 Å by using the program DENZO/SCALEPACK (21). Intensities were converted to structure factors by using the method of French and Wilson (22) as implemented in the program TRUNCATE in the CCP4 suite of programs (23).

Solution Characterization. Sedimentation equilibrium andguanidine HCl denaturation (in 0.01 M Mes buffer (pH 6.5), 0.1 M NaCl) was conducted as described (20). Thermal denaturation curves between 2 and 94°C were monitored by measuring the ellipticity at 222 nm in the circular dichroism (CD) spectrum of the proteins. The concentration of Mon1 was 25 μM and the curves measured in the presence of guanidine hydrochloride (Gdn·HCl), ranging from 0 to 2 M. Thermal unfolding curves for 35 μM DSD were measured at concentrations of Gdn·HCl ranging from 0 to 5.5 M. The data at intermediate Gdn·HCl concentrations were analyzed globally by using the Gibbs Helmholtz equation (24), adapted for a monomer/dimer equilibrium.

Results

Sequence Design. The design of DSD and DSAg followed well-known principles of protein design, which have been used in the construction of three-helix bundles based on coil-Ser. To simplify the synthesis and modeling, the helices in the target structures were shortened to two heptads, as compared with three heptads in earlier designs. The helices were connected by loops to provide two bundles differing in topology, designated Mon1 and Mon2. The above considerations suggest that a domain-swapped up-down-up three-α-helix bundle will form a closed, dimeric structure, whereas an up-down-down construct will tend to form open, fibrous oligomers. To test this hypothesis, we designed domain-swapped three-helix bundles with up-down-up (DSD) and up-down-down (DSAg) topologies, as well as their monomeric counterparts (Mon1 and Mon2). In each case, the hydrophobic cores of these proteins consist exclusively of leucine side chains. The connecting Loop 1 sequence is intended to adopt a four-residue, right-handed interhelical loop, with a $\gamma-\alpha_L-\beta-\beta$ main chain conformation (25). The loop included a hydrophobic residue (Phe17), intended to cap the hydrophobic core of the bundle. The precise positions of charged glutamates and lysines at *e* and *g* positions of the helical heptads were selected to stabilize electrostatically the desired topology and to destabilize various alternatives. For example, the DSAg sequence should have more favorable electrostatic interactions in an oligomeric up-down-down topology, relative to the dimeric up-down-up structure (Fig. 2). Comparison of the sequences of DSAg and DSD (Fig. 1*C*) shows that all hydrophobic core residues are conserved, with only six of the charged residues exchanged. Thus, neglecting charged residues, DSAg and DSD can be viewed as the same protein in two alternative 3D domain-swapped forms: open-ended and extended for DSAg and closed and dimeric for DSD. Although the DSD and DSAg comprise the primary focus of this work, we also prepared Mon1 to establish that a three-helix bundle with relatively short helices could indeed adopt a monomeric, folded helical structure, and also to provide a standard for comparison with the domain-swapped structures.

Analytical Ultracentrifugation. The aggregation state of Mon1, DSD, and DSAg were examined by using equilibrium analytical ultracentrifugation at concentrations of 100, 250, and 500 μM in 0.05 Mes buffer (pH6.5), 0.1 M NaCl. The data for Mon1 were analyzed assuming a single, noninteracting molecular species, yielding an apparent molecular weight in excellent agreement with that expected for a monomer (4,900 vs. 4,920 Da, respectively). At a loading concentration of 0.1 mM and lower, DSD sedimented as a single species with an apparent molecular weight of 10,900, in good agreement with that expected for a dimer (10,500 Da). Thus, the protein adopts a very stable dimer, which does not appreciably dissociate under these conditions. The DSAg protein tended to form insoluble aggregates at long times. However, the portion of the protein that remained in solution showed an apparent molecular weight of 15,100, which is larger than that expected for a dimer (10,500). Thus, this protein tended to form higher order aggregates, although its tendency to associate precluded a detailed analysis.

Thermodynamics of Folding. Mon1, DSD, and DSAg were highly helical as assessed by CD spectroscopy (mean residue ellipticity, $[\theta_{222}]$ = 22,500 ± 1,500 deg cm^2·dmol^{-1}, 24,500 ± 1,500 deg cm^2·dmol^{-1}, and 28,500 ± 1,500 deg cm^2·dmol^{-1}, respectively). The thermodynamic stabilities of DSD and Mon1 were obtained by measuring the variation of $[\theta_{222}]$, as a function of temperature

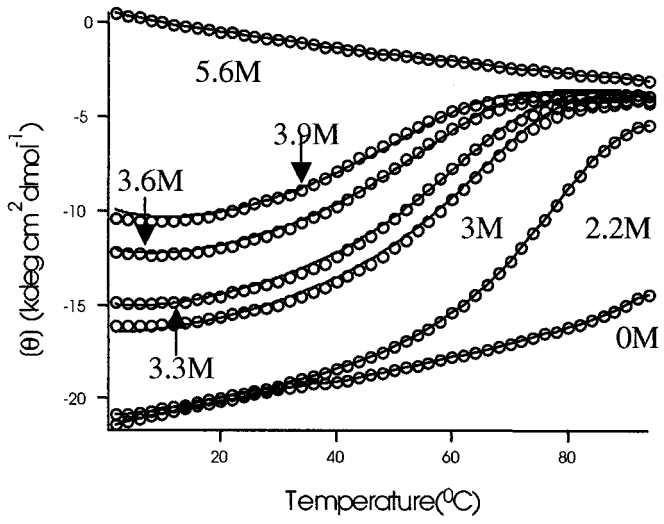

Fig. 3. Thermal denaturation of DSD. CD data monitoring the loss of helical signal at 222 nm with increasing temperature at varying concentrations of Gdn·HCl: 0 M, 2.19 M, 3 M, 3.3 M, 3.6 M, 3.9 M, and 5.6 M, respectively. The smooth lines represent theoretical curves obtained by using parameters from the fitting procedure (see *Materials and Methods*).

at various concentrations of guanidine HCl. Because the hetereogeneity in the aggregation state of DSAg would render a rigorous thermodynamic analysis very difficult, the stability of this protein was not evaluated. The thermal denaturation curves for Mon1 are very similar to those described previously for α_3D, a three-helix bundle based on Coil-Ser (13), showing high- and low-temperature-induced folding transitions. However, as would be expected from its very small size, the folding of Mon1 is considerably less favorable. The thermodynamic parameters obtained from a global analysis of the curves provides $\Delta Cp = 0.235 \pm 0.03$ Kcal mol^{-1}·deg^{-1}, $\Delta H^0 = 7.8$ Kcal/mol, and $T_M = 52$°C. The free energy of folding, evaluated at room temperature, was 0.5 Kcal/mol.

The thermal and guanidine-dependent unfolding curves for DSD were concentration dependent, indicating that folding and dimerization were thermodynamically linked. The dissociation constant for dimerization of DSD was determined to be 140 pM by global analysis of the guanidine denaturation curves at two peptide concentrations, 2.7 μM and 13.3 μM. In contrast to Mon1, DSD is extremely resistant to thermal denaturation: it is 80% folded at 94°C. Thermal unfolding studies, conducted at various concentrations of guanidine HCl (Fig. 3), provided values of $\Delta H^0 = 70.5$ Kcal/mol, $\Delta Cp = 0.68 \pm 0.04$ Kcal mol^{-1}·deg^{-1}, and T_M 105°C at 0 M Gdn (standard state, 100 μM). Comparisons of unimolecular and bimolecular processes are fraught with difficulties associated with the choice of an appropriate standard state. Nevertheless, it is apparent that DSD is much more resistant to thermal and guanidine denaturation than the corresponding monomeric derivative, Mon1, at all experimentally accessible protein concentrations. The enhanced stability of the structure is consistent with the larger structure and more extensive burial of hydrophobic groups in DSD.

Structural Characterization of DSD. DSD was crystallized and its structure determined by x-ray diffraction. Phases were found by

Table 1. Data collection, phasing, and refinement statistics for the DSD

Data collection and phasing	Native (room temperature)	Native (cryo)	$HgCl_2$	PIP	$K_3UO_2F_5$
Resolution, Å	32.6–2.1	28.6–1.5	32.6–2.9	32.6–2.4	29.2–2.9
Reflections, I/s > 0 (unique)	25,629 (5,532)	80,427 (14,635)	6,485 (2,183)	24,124 (3,808)	7,124 (2,167)
Completeness, % (high resolution shell, %)*	99.1 (98.7)	99.2 (94.1)	99.0 (100.0)	99.8 (100.0)	99.1 (99.5)
R_{merge} (%)†	8.0 (28.9)	8.2 (27.9)	9.9 (31.6)	10.4 (25.5)	10.5 (29.7)
R_{scale}, %‡	—	—	29.6	18.7	14.4
Phasing Power§	—	—	0.71 (0.4)	1.12 (1.34)	1.16 (1.16)
R_{cullis}¶	—	—	0.58	0.48	0.44
No. of binding sites	—	—	2	2	3
Figure of Merit:	0.59 for 10–3.1 Å				
Refinement Statistics					
R-factor, %	19.9				
R_{free}, %‖	24.1				
Rms bonds	0.018 Å				
Rms angles	1.8°				
Rms dihedrals	16.0°				

X-ray data collection, phasing, and refinement statistics. Crystals were grown from purified DSD in the cubic space group $P2_13$, with room temperature cell parameters a = b = c = 65.24 Å, $\alpha = \beta = \gamma = 90°$. Three heavy atom derivatives, Hg, Pt, and U, were used to determine phases, which were refined by using SOLVE (26). Initial MIR maps were calculated by using the program FFT from the CCP4 suite of programs (23). These maps were improved by applying the solvent flattening procedure from the program DM (27) where α-helical density was clearly identified. In subsequent rounds of refinement in XPLOR (28), the complete sequence was built into model-phased, SIGMAA-weighted electron density maps (29). A bulk solvent correction protocol (30) was applied to the structure factors in the resolution range from 30–1.5 Å and used throughout refinement. Map display and model building was performed in the program O (31). R_{free} was monitored in each round of refinement to avoid overfitting (32). To verify the quality of the model, simulated annealing omit maps (29, 33) were calculated in which six contiguous residues at a time were omitted in the phase calculation (one residue overlap). The present model includes 718 protein atoms, 85 waters, one sulfate ion, and one molecule tentatively modeled as trifluoracetic acid.

*Completeness calculated in the highest resolution shell. For the room temperature native data set, the high resolution shell was from 2.10–2.18 Å; for the cryo native, 1.49–1.54 Å; for the $HgCl_2$, 2.90–3.0 Å; for PIP, 2.4–2.49 Å; for $K_3UO_2F_5$ 2.90–3.0 Å.

†$R_{merge} = \Sigma_{hkl}|I_i - \langle I\rangle|/\Sigma_{hkl} I_i$; conventional discrepancy R-factor for scaling intensities I.

‡$R_{scale} = \Sigma_{hkl}|I - I_P|/\Sigma_{hkl}|I_P|$, where $|I_P|$ is taken from the room temperature native dataset.

§Phasing power is the rms isomorphous difference over the rms residual lack of closure for accentric and (centric) reflections. Phasing power = $\Sigma_{hkl}|F_H|/\Sigma_{hkl}|F_{PH,obs}| - |F_{PH,calc}|$.

¶$R_{cullis} = \Sigma_{hkl}(\|F_{PH} \pm F_P| - F_{Hcalc}|)/\Sigma_{hkl}|F_{PH} \pm F_P|$.

‖$R_{free} = \Sigma_{hkl} \| F_o | - | F_c| / \Sigma_{hkl} |F_o|$ for a test set of 10% of all reflections.

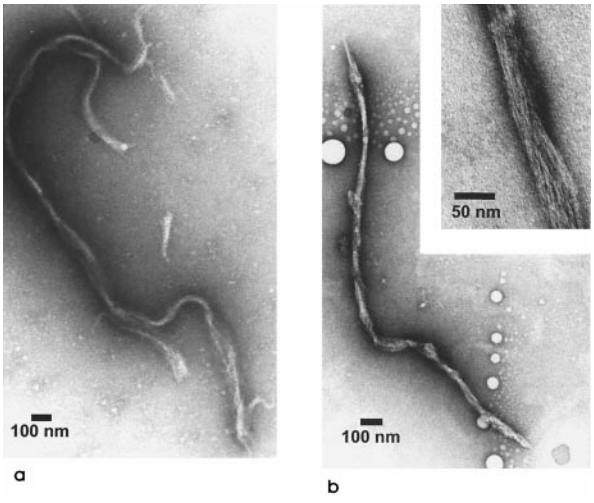

Fig. 4. Electron micrographs of the DSAg fibrils. (*a*) DSAg at neutral conditions (pH 6.5) under ×70,000 magnification. (*b*) DSAg at acidic conditions (pH 2.4) under ×70,000 magnification. The *Inset* is shown at ×276,000 magnification. Notice the fibril is composed of several protofibrils.

multiple isomorphous replacement and the structure was refined to 1.5 Å (Table 1). The structure, as designed, forms a 3D DSD (Fig. 1*A*). Most of the features designed into the DSD sequence to stabilize the 3D DSD are confirmed by the crystal structure. Residues 1a–14a, 19a–48a (monomer A), 1b–13b, and 19b–48b (monomer B) are α-helical. The hairpin loops corresponding to residues 15a–18a and 14b–18b form turns connecting domains I and II of each monomer. The loop conformation is similar to that of the design, and Phe17a and Phe17b cap the hydrophobic core of the bundle. Nine of the 12 designed *e–g* salt bridges are formed between adjacent monomers in the structure of DSD. The glutamates and lysines in the remaining *e* and *g* positions that do not form salt bridges to adjacent monomers within the DSD interact electrostatically with adjacent symmetry-related monomers related by a crystallographic three-fold axis.

It is noteworthy that the N termini of the two short helices in DSD abut in the structure of the DSD. The partial positive charges associated with the N termini of these helices are focused within a small, 5-Å cleft as in natural proteins, which use similarly oriented helices to bind anionic substrates (34). Thus, DSD may have attractive possibilities for the evolution of novel binding functionalities.

Structural Characterization of DSAg. The design of DSAg calls for the *e–g* electrostatic interactions to orient open monomers into a fibrous oligomer containing an indefinite number of molecules, instead of an oligomer that stops at the level of a dimer, as in the case of DSD. Because of the difficulty in crystallizing fibrous proteins, we used negative staining electron microscopy, dynamic light scattering, CD spectroscopy, and Fourier transform-IR spectroscopy to characterize DSAg.

At both acidic and neutral pH, electron micrographs show that DSAg forms long fibrous aggregates (Fig. 4). The DSAg fibrils are 40–70 nm in width and up to several thousand nm in length. A structural hierarchy is seen in the micrographs where the fibrils are composed of several protofibrils, corresponding approximately to the thickness of one to three triple-stranded α-helical bundles as seen in the crystal structure of DSD. The protofibrils are thus consistent with the dimensions of the designed DSAg fibril. In turn, each α-helix of the three-α-helical bundle can be thought of as a subprotofibril, having the width of 10–15 Å expected for a single α-helix. At acidic pH (pH 2.4) fibrils of DSAg are also clearly seen by negative staining electron microscopy (EM) (Fig. 4*b*), even though at this low pH, many of the glutamates at *e/g* heptad positions would be expected to be protonated.

For comparison, we also examined solutions of DSD by negative staining EM. Near neutral pH (pH 6.5) no fibrils of DSD were seen, however, some globular aggregates were observed. At acidic pH (pH 2.4), solutions of DSD formed small amorphous aggregates, but no long fibrils were observed.

Dynamic light scattering experiments on solutions of DSAg, prepared with the same buffer conditions as our EM samples, showed the presence of large molecular weight species: the calculated radii of hydration ranged from 30–80 nm—within the range of particles seen by EM. Although the light scattering experiments cannot easily distinguish between fibrous aggregates and amorphous aggregates, the electron micrographs suggest that the large species seen in the light scattering experiments are indeed fibrils. We conclude that DSAg, designed to form fibrils, does form fibrils, with each fibril composed of several protofibrils of diameter comparable to the three-α-helical bundle of the design.

The DSAg protein is α-helical, as judged by infrared spectroscopy (Fourier transform-IR), showing an amide I′ band characteristic of coiled coils (35, 36). Both in solution (20 mg/ml in D_2O 0.01 M phosphate buffer (pH 6.6) with 0.1 M NaCl) and following evaporation onto a CaF_2 plate, a peak centered at 1640 cm^{-1} was observed, and the spectra were devoid of peaks characteristic of β-structure. We conclude that the fibrous aggregates of DSAg are α-helical, as designed.

Discussion

The small size of the designed proteins and their well-studied motif—coiled coils—has enabled us to probe the features required for the design of open oligomeric structures as opposed to closed dimers. These designed molecules demonstrate that domain swapping can give rise either to dimers or higher-order oligomers, depending on the topology of the original, monomeric bundle. The atomic structure of the linkages between molecules in DSAg is not known directly from experiments, but there are strong reasons to think it is the 3D domain-swapped three-α-helical bundle of the design (Fig. 1*B*). First, the closely related design of DSD is confirmed by x-ray crystallography to be a 3D domain-swapped three-α-helical bundle. Second, the functional unit designed into the fibril is chemically identical (with an identical hydrophobic core) to that found in DSD. Third, the design of DSAg would be expected to produce a fibril through the pattern of continued 3D domain swapping. During elongation of the fibril, each new functional unit is covalently connected to the previous functional unit, and yet maintains the chemically identical noncovalent interactions observed in the structure of DSD. These results support the hypothesis that 3D domain swapping can lead to fibril formation.

The ability to design synthetic fibrous proteins offers the possibility of making self-assembling biomaterials with defined properties for various applications. Because the structural basis of the interaction in the DSAg fibril is established, more elaborate versions could be tailored with other physical characteristics by altering the amino acid sequence to exploit hydrogen bonding, π stacking, and electrostatic forces. It could then be possible to engineer fibrils with defined thickness, tensile strength, solubility, and adhesion strength, as has been done in the engineering of artificial hydrogels (37), silk-like proteins (38), and other fibrous aggregates (39). One potential biotechnological application could be protein recruitment, noting that the head-to-tail packing of the DSAg oligomer is reminiscent of the packing between PDZ domains of the nNOS-Syntrophin signaling complex (40). Furthermore, functional groups could be added to the surface of the repeating protein unit, permitting the fibrous protein to serve as a vehicle for drug localization and deposition. Thus the DSAg fibril illustrates the use of a specific

interaction—3D domain swapping—for the design of a new class of fibrous proteins, and can serve as a prototype for future designs of self-assembling fibrous polymers.

We thank Dr. Malcolm Capel for help at National Synchrotron Light Source Beamline X12B, Dr. Duilio Cascio, and Dr. Daniel Anderson for discussions. This research was supported by the National Institutes of Health Chemistry/Biology Interface Predoctoral Training at the University of California, Los Angeles (GM-54616 to W.F.D.; N.L.O. was a trainee supported by this grant), the Materials Research Science and Engineering Center program of the National Science Foundation (DMR96-32598 to W.F.D.), and the National Science Foundation (MCB 94-29768 to D.E.).

1. Schlunegger, M. P., Bennett, M. J. & Eisenberg, D. (1997) *Adv. Protein Chem.* **50,** 61–122.
2. Bennett, M. J., Choe, S. & Eisenberg, D. (1994) *Proc. Natl. Acad. Sci. USA* **91,** 3127–3131.
3. Klafki, H.-W., Pick, A. I., Pardowitz, I., Cole, T., Awni, L. A., Barnikol, H. V., Mayer, F., Kratzin, H. D. & Hilschmann, N. (1993) *Biol. Chem. Hoppe-Seyler* **372,** 1117–1122.
4. Carroll, S. F., Barbieri, J. T. & Collier, R. J. (1988) *Methods Enzymol.* **165,** 68–76.
5. Gotte, G., Testolin, L., Costanzo, C., Sorrentino, S., Armato, U. & Libonati, M. (1997) *FEBS Lett.* **415,** 308–312.
6. Crestfield, A. M., Stein, W. H. & Moore, S. (1962) *Arch. Biochem. Biophys.*, Suppl. 1, 217–222.
7. Hodges, R. S., Sodek, J., Smillie, L. B. & Jurasek, L. (1972) *Cold Spring Harbor Symp. Quant. Biol.* **37,** 299–310.
8. Lovejoy, B., Choe, S., Cascio, D., McRorie, D. K., DeGrado, W. F. & Eisenberg, D. (1993) *Science* **259,** 1288–1293.
9. O'Neil, K. T. & DeGrado, W. F. (1990) *Science* **250,** 646–651.
10. McLachlan, A. D. & Stewart, M. (1975) *J. Mol. Biol.* **98,** 293–304.
11. Johansson, J., Gibney, B., Skalicky, J., Wand, A. & Dutton, P. (1998) *J. Am. Chem. Soc.* **120,** 3881–3886.
12. Walsh, S. T. R., Cheng, H., Bryson, J. W., Roder, H. & DeGrado, W. F. (1999) *Proc. Natl. Acad. Sci. USA* **96,** 5486–5491.
13. Bryson, J. W., Desjarlais, J. R., Handel, T. M. & DeGrado, W. F. (1998) *Protein Sci.* **7,** 1404–1414.
14. Lumb, K. J. & Kim, P. S. (1995) *Biochemistry* **34,** 8642–8648.
15. Dickason, R. R. & Huston, D. P. (1996) *Nature (London)* **379,** 652–655.
16. Green, S. M., Gittis, A. G., Meeker, A. K. & Lattman, E. E. (1995) *Nat. Struct. Biol.* **2,** 746–752.
17. Pei, X. Y., Holliger, P., Murzin, A. G. & Williams, R. L. (1997) *Proc. Natl. Acad. Sci. USA* **94,** 9637–9642.
18. Raag, R.& Whitlow, M. (1995) *FASEB J.* **9,** 73–80.
19. Liu, Y., Hart, P. J., Schlunegger, M. P. & Eisenberg, D. (1998) *Proc. Natl. Acad. Sci. USA* **95,** 3437–3442.
20. Ghirlanda, G., Lear, J. D., Lombardi, A. & DeGrado, W. F. (1998) *J. Mol. Biol.* **281,** 379–391.
21. Otwinowski, Z. & Minor, W. (1996) in *Methods in Enzymology*, eds. Carter, J. C. W. & Sweet, R. M. (Academic, London), Vol. 276, pp. 307–325.
22. French, S. & Wilson, K. (1978) *Acta Crystallogr. A* **34,** 517–525.
23. The CCP4 Suite: Programs for Protein Crystallography (1994) *Acta Crystallogr. D* **50,** 760–763.
24. Kuhlman, B. & Raleigh, D. P. (1998) *Protein Sci.* **7,** 2405–2412.
25. Efimov, A. V. (1991) *Protein Eng.* **4,** 245–250.
26. Terwilliger, T. C. & Berendzen, J. (1999) *Acta. Crystallogr. D* **55,** 849–861.
27. Cowtan, K. (1994) *Joint CCP4 and ESF-EACBM Newsletter on Protein Crystallography* **31,** 34–38.
28. Brünger, A. T. (1988) in *Crystallographic Computing 4: Techniques and New Technologies*, eds. Isaacs, N. W. & Taylor, M. R. (Clarendon, Oxford), pp. 126–140.
29. Read, R. J. (1986) *Acta Crystallogr. A* **42,** 140–149.
30. Jiang, J. S. & Brunger, A. T. (1994) *J. Mol. Biol.* **243,** 100–115.
31. Jones, T. A., Zou, J. Y., Cowan, S. W. & Kjelgard, M. (1991) *Acta Crystallogr. A* **47,** 110–119.
32. Brunger, A. T. (1992) *Nature (London)* **355,** 472–474.
33. Hodel, A., Kim, S.-H. & Brunger, A. (1992) *Acta Crystallogr. A* **48,** 851–859.
34. Hol, W. G. J. (1985) *Prog. Biophys. Mol. Biol.* **45,** 149–155.
35. Reisdorf, W. C., Jr., & Krimm, S. (1996) *Biochemistry* **35,** 1383–1386.
36. Heimburg, T., Schunemann, J., Weber, K. & Geisler, N. (1999) *Biochemistry* **38,** 12727–12734.
37. Petka, W. A., Harden, J. L., McGrath, K., Wirtz, P. D. & Tirrell, D. A. (1999) *Science* **281,** 389–392.
38. Cappello, J., Crissman, J. W., Crissman, M., Ferrari, F. A., Textor, G., Wallis, O., Whitledge, J. R., Zhou, X., Burman, D., Aukerman, L., *et al.* (1997) *J. Controlled Release* **53,** 105–117.
39. Engelkamp, H., Middelbeek, S. & Nolte, R. J. M. (1999) *Science* **284,** 785–788.
40. Hillier, B. J., Christopherson, K. S., Prehoda, K. E., Bredt, D. S. & Lim, W. A. (1999) *Science* **284,** 812–815.